Modelling and simulation of dynamic wheel-rail interaction using a roller rig

A Anyakwo, C Pislaru, A Ball and F Gu
Centre for Diagnostic Engineering, University of Huddersfield, Queensgate, Huddersfield HD1 3DH, United Kingdom

Email: arthur.anyakwo@hud.ac.uk

Abstract. The interaction between the wheel and rail greatly influences the dynamic response of railway vehicles on the track. A roller rig facility can be used to study and monitor real time parameters that influence wheel-rail interaction such as wear, adhesion, friction and corrugation without actual field tests being carried out. This paper presents the development of the mathematical models for full scale roller rig and 1/5 scale roller rig and the wear prediction model based on KTH wear function. The simulated critical speed for the 1/5 scale roller rig is about one-fifth of the critical speed for the full scale model so the simulated results compare well with the theory related to wheel-rail contact and dynamics. Also the differences between the simulated rolling radii for the full scale model with and without wear function are analysed. This paper presents the initial stage of a large scale research project where the influence of wear on the wheel-rail performance will be studied in more depth.

1. Introduction

Modelling and simulation of wheel-rail interaction using a scale roller rig is necessary for better understanding of dynamic behaviour of the railway vehicle in a controlled laboratory environment less prone to noise and disturbances. Applications of roller rigs include vehicle stability tests, track irregularities, ride comfort, wheel-rail interaction, wear, rolling contact fatigue.

Raising performance needs and increased importance on scheduled maintenance and life cycle costs for railway vehicles and tracks, have attracted interest to the necessity of predicting wheel and rail wear by simulation. Developing a wear prediction model enables railway researchers to better understand wear mechanisms and its effect on the dynamic behaviour of the system so that re-profiling of the wheels-rails can be easily carried out without planned maintenance schedules. It also helps in improvements in wheel design and materials in order to reduce wear. For enhanced understanding of the phenomena, roller rigs are can be used to simulate wheel wear and its effects of the railway vehicle dynamics.

Hur et al [1] studied the influence of wheel profile wear on scale bogie stability using critical speed tests. The numerical models for full scale roller rig and 1/5th scale rig contained the wheel-rail contact models (including the wear parameters – flange thickness, flange height, wear factor and flange contact angle) were implemented in MATLAB. Four dynamic tests with various critical speeds were performed and the wear parameters were determined from the wheel profiles measured with mini-prof. The critical speeds for the full scale test rig were inversely proportional to equivalent conicity of the wheel profile (which increased with the wheel flange wear). This work is one of the major works carried out on wheel wear for scale roller rig applications. Allen et al [2] used a roller rig to investigate the dynamic behaviour of railway vehicles. He computed the critical velocity of the roller rig and compared the same results with simulations of a full scale roller rig. Errors found in simulation results where as a result of scaling and correlation reduction between scale roller rigs and full-scale vehicles.

Pombo et al [3] developed a wear prediction tool for railway wheels using three different wear functions: British Rail Research (BRR) Wear function, KTH wear function and University of Sheffield (USFD) wear function.

- BRR wear function relates the lost material from the wheel-rail to the product of the tangential contact force (T) and the global creepage (β). So the contact stress and creepage are related to the wear when wheel tread wear and mile regime are considered.
- KTH wear function [4] is based on Archard's wear law were the volume of worn material is directly proportional to the normal contact force (N), the sliding distance (S) and the wear coefficient (k) and is inversely proportional to the hardness of the material (H). It is important to note that the wear coefficient parameter k depends on slip velocity and the normal contact pressure of the contact area. The advantage of using the KTH function is that the volume of wear and the wear depth can be computed locally and globally. The main drawback of this function is that it is time consuming.
- USFD wear function [3] states that the wear rate is proportional to the production of the wear constant K and wear index Tβ, and inversely proportional to the contact area (A) of the wheel-rail contact patch. The main disadvantage of the method is that the local wear computation is cumbersome since additional time is required to compute it.

This paper presents the development of the mathematical models for full scale roller rig and 1/5 scale roller rig and the wear prediction model based on KTH wear function. Also the simulated results after these models are implemented in MATLAB are analysed. Section two explains the development of full scale roller rig model using Heuristic non-linear creep method. The simulated results for wheel-rail profiles, contact point positions, radius difference function, contact angle function and equivalent conicity are discussed in Section three. The evaluation of wheel-rail contact forces and wheelset suspension forces is performed in Sections four respectively five. The development of 1/5 scale roller rig model is explained in Section six. The simulated dynamic behaviour of 1/5 scale roller rig model and full scale roller rig model are analysed in Section seven. The wear modelling based on Archard's wear model is presented in the next section. The differences between the simulated rolling radii for the full scale model with and without wear function are discussed in the final section.

2. Development of full scale roller rig model

The non-linear differential equations of motion used to simulate the dynamic model of a typical bogie are expressed in Equations (1 – 6). The bogie frame and the wheelset are allowed to move in the yaw and lateral directions. The creep forces developed at the contact points were determined using FASTSIM algorithm [7]. The equations of motion are expressed as follows:

.

$$m\frac{d^2y_1}{dt^2} = F_{yr1} + F_{yl1} + N_{ry1} - N_{ly1} + F_{susp1} \quad (1)$$

$$m\frac{d^2y_2}{dt^2} = F_{yr2} + F_{yl2} + N_{ry2} - N_{ly2} + F_{susp2} \quad (2)$$

$$I_z\frac{d^2\psi_1}{dt^2} = -l_o(F_{xl1} - F_{xr1}) + (R_{rx1} + R_{rr1}) * \left(F_{yr1} + N_{ry1}\right) - (R_{lx1} + R_{ll1})(F_{yl1} + N_{ly1}) \quad (3)$$

$$I_z\frac{d^2\psi_2}{dt^2} = -l_o(F_{xl2} - F_{xr2}) + (R_{rx2} + R_{rr2}) * \left(F_{yr2} + N_{ry2}\right) - (R_{lx2} + R_{ll2})(F_{yl2} + N_{ly2}) \quad (4)$$

$$m_b\frac{d^2y_3}{dt^2} = F_{susp1} + F_{susp2} \quad (5)$$

$$I_b\frac{d^2\psi_3}{dt^2} = b(F_{susp1} + F_{susp2}) - (M_{susp1} + M_{susp2}) \quad (6)$$

where:

m = mass of the wheelset (kg)
m_b = mass of Bogie frame (kg)
I_z = Yaw moment of inertia of wheelset (kgm^2)
I_b = Yaw moment of inertia of the Bogie frame (kgm^2)
y_1 = Lateral displacement of wheelset 1 (m)
y_1 = Lateral displacement of wheelset 2 (m)
I_b = Yaw moment inertia of the Bogie frame (kgm^2)
y_1 = Lateral displacement of wheelset 1 (m)
y_1 = Lateral displacement of wheelset 2 (m)
ψ_1 = Yaw displacement of wheelset 1 (radians)
ψ_2 = Yaw displacement of wheelset 2 (radians)
F_{xr1} = Longitudinal creep force of right wheel 1 (N)

ψ_1 = Yaw displacement of wheelset 1 (radians)
ψ_2 = Yaw displacement of wheelset 2 (radians)
F_{xr1} = Longitudinal creep force of right wheel 1 (N)
F_{xl1} = Longitudinal creep force of left wheel 1 (N)
F_{xr2} = Longitudinal creep force of right wheel 2 (N)
F_{xl2} = Longitudinal creep force of left wheel 2 (N)
F_{yr1} = Lateral contact force of right wheel 1 (N)
F_{yl1} = Lateral contact force of left wheel 1 (N)
I_b = Bogie frame Yaw moment of inertia of the Bogie frame (kgm^2)
y_1 = Lateral displacement of wheelset 1 (m)
y_1 = Lateral displacement of wheelset 2 (m)
ψ_1 = Yaw displacement of wheelset 1 (radians)
ψ_2 = Yaw displacement of wheelset 2 (radians)
M_{susp2} = Suspension moment wheelset 2 (N)
l_o = Half wheelset gauge (mm)
R_{rx1} = Longitudinal contact position right wheel 1 (m)
R_{rx2} = Longitudinal contact position right wheel 2 (m)
R_{lx1} = Longitudinal contact position left wheel 1 (m)
Rl_{x2} = Longitudinal contact position left wheel 2 (m)

F_{xl1} = Longitudinal creep force of left wheel 1 (N)
F_{xr2} = Longitudinal creep force of right wheel 2 (N)
F_{xl2} = Longitudinal creep force of left wheel 2 (N)
F_{yr1} = Lateral contact force of right wheel 1 (N)
F_{yl1} = Lateral contact force of left wheel 1 (N)
F_{yr2} = Lateral contact force of right wheel 2 (N)
F_{yl2} = Lateral contact force of left wheel 2 (N)
M_{zr1} = Spin creep moment of right wheel 1 (N)
M_{zl1} = Spin creep moment of left wheel 1 (N)
M_{zl2} = Spin creep moment of left wheel 2 (N)
F_{susp1} = Suspension force wheelset 1 (N)
F_{susp2} = Suspension force wheelset 2 (N)
M_{susp1} = Suspension moment wheelset 1 (N)
N_{ry1} = Lateral normal contact force right wheel 1 (m)
N_{ry2} = Lateral normal contact force right wheel 2 (m)
N_{ly1} = Lateral normal contact force left wheel 1 (m)
Nl_{y2} = Lateral normal contact force left wheel 2 (m)
b = wheelset base

3. Simulated results for wheel-rail contact geometry

The wheel-rail geometry was obtained from new P8 wheel and BS 110A rail profiles. No cant was applied to the rail profile. For the roller rig, the wheel and roller profiles are scaled down based on one-fifth of the actual wheel-rail profile. The full scale wheel-roller profiles are shown in figure 1.

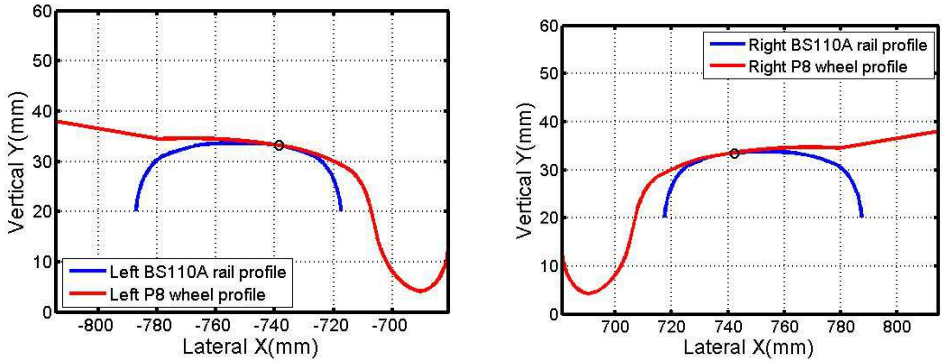

(a) Left wheel-rail profiles (b) Right wheel-rail profiles

Figure 1. Simulated left and right wheel-rail profiles for full scale model.

The contact point locations were determined using two dimensional wheel-rail geometry analysis where the lateral displacement and the roll angle are used as inputs. The locations of the contact points on the wheel and the rail where determined by solving the geometrical constraint equations arising from the profile geometry. The contact point locations obtained on the left and right rail profiles for a positive lateral displacement is shown in figure 2.

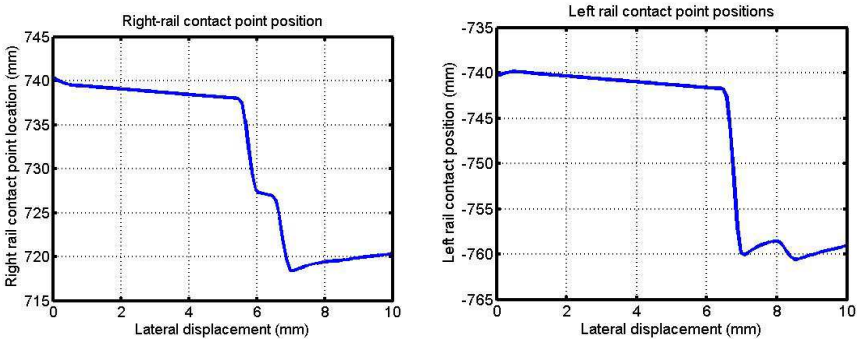

(a) Right rail contact point positions (b) Left rail contact positions

Figure 2. Simulated right and left contact positions for full scale model.

As can be observed from figure 2, there is lack of symmetry in both left and right contact point locations due to the positive lateral displacement of the wheelset from 0 to 10mm. This implies that for a given lateral excursion on the left and right rail profiles, the movement of these contact point locations would differ.

Functions derived from the wheel-rail/roller geometry include the rolling radius difference function, the contact angle and the equivalent conicity. The rolling radius function (figure 3) is proportional to the rate of change of the lateral displacement.

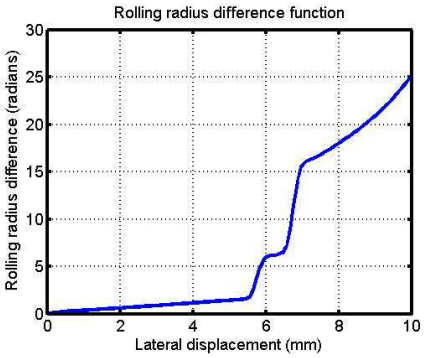

Figure 3. Simulated rolling radius difference function for full scale model.

At 5.5mm, the wheelset flange makes the first contact with the rail gauge. The sharp contact jump experienced at the wheel flange contact is due to the increase in the lateral displacement of the wheelset. Further increase of the lateral displacement leads to an increase in the rolling radius difference and thus could lead to derailment

The contact angle function is derived from the derivative of the rail lateral contact co-ordinate function with respect to the lateral displacement and the simulated results are shown in figure 4.

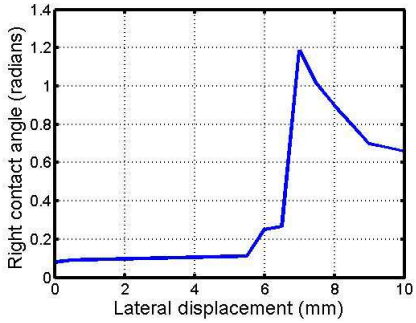

Figure 4. Simulated contact angle function for full scale model.

At 7 mm the contact angle is very large and it reaches about 1.18 radians (68 degrees). This is due to the fact that the flange angle of the wheel profile is about 1.18 radians and the wheelset has reached the flange region. The contact angle should decrease when the lateral displacement is increasing further on so wheelset remains in the central position.

The equivalent conicity function (figure 5) is an approximation that accounts for the average slope of the rolling radius difference function over a finite range of the lateral displacement of the wheelset on the rail. Given that the rolling radius difference function is expressed as follows:

$$R(y) = 2\lambda y \tag{7}$$

Where R(y) is the rolling radius difference function, λ is the effective conicity and y is the lateral displacement, the equivalent conicity calculated via the trapezoidal rule can be expressed as follows:

$$\lambda_e = \frac{1}{4\Delta y^2}\int_{-\Delta y}^{\Delta y} R(y)dy \tag{8}$$

where the lateral displacement range is from -Δy to + Δy [6].

For the 1/5 scaled roller rig, the wheel-roller contact geometry parameters are scaled down and used for dynamic simulations of the wheel-rail contact model.

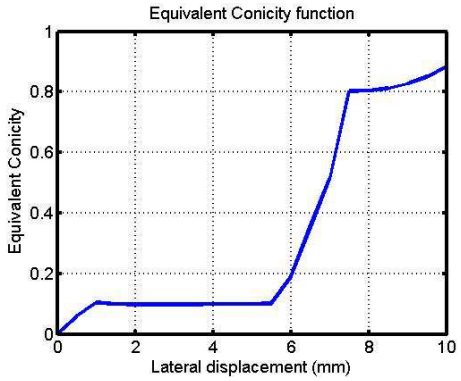

Figure 5. Simulated equivalent conicity function for full scale model.

4. Evaluation of wheel-rail contact forces

Wheel-rail contact forces are developed as a result of creepages emanating from the contact patch. These creepages arise as a result of traction, braking, acceleration due to the relative motion of the wheel on the rail. The creep forces developed as a result are the lateral, longitudinal and spin moment creep forces. The computation of the wheel-rail/roller contact forces was carried out using FASTSIM algorithm proposed by Kalker. The contact patch (assumed to be elliptical) was divided into several rectangular grids using. An 81 x 81 (m x n) grid with a and b as semi-axes dimensions was used for the simulation purposes so the creep forces can be calculated with increased accuracy. The values for the contact stress were determined for every point from the rectangular grid and compared with the traction bound. Adhesion occurs if the surface traction forces is less than or equal to the traction bound while slip occurs only when the surface traction is greater than the traction bound. Finally the lateral and longitudinal creep forces of the left and right wheel-rail contact were obtained by summing the surface tractions forces in the lateral and longitudinal direction. The block diagram showing the implementation of the algorithm is shown below:

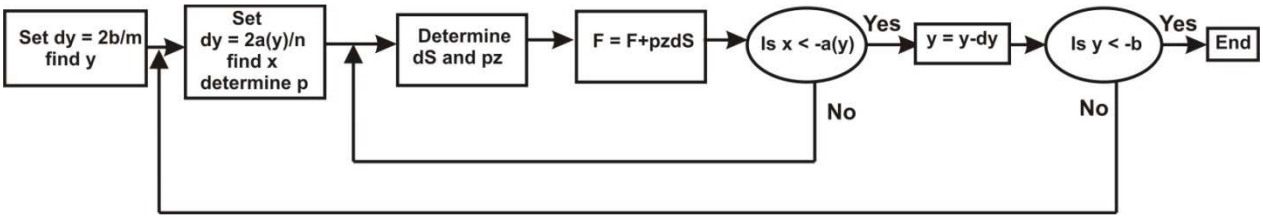

Figure 6. Steps for implementation of FASTSIM Block diagram.

Where a(y) is the x bound of the contact patch in the longitudinal direction, x and y are the co-ordinates located inside the elliptical contact patch, dS is the area of each element in the grid, and pz is the surface traction resolved in the longitudinal and lateral direction respectively.

5. Calculation of wheelset suspension forces

The suspension forces influence the dynamic behaviour of the 1/5 scaled roller rig and real railway vehicle bogie on the track. The suspension forces on wheelset 1 respectively wheelset 2 are:

$$F_{susp1} = -2K_{py}(-y_1 + y_b - b\psi_b) - 2\dot{C_{py}}(-\dot{y}_1 + \dot{y}_b - b\dot{\psi}_b) \quad (9)$$

$$F_{susp2} = -2K_{py}(-y_2 + y_b + b\psi_b) - 2\dot{C_{py}}(-\dot{y}_2 + \dot{y}_b + b\dot{\psi}_b) \quad (10)$$

where K_{py}/C_{py} is the lateral stiffness/lateral damping of the spring. y_1 and y_2 are the lateral displacement of the front and rear wheelsets respectively. y_b is the lateral displacement of the bogie, and ψb and $\dot{\psi}_b$, are the yaw angle bogie and yaw velocity of the bogie respectively. $\dot{y}_1$, $\dot{y}_2$ and $\dot{y}_b$ are the lateral velocity of the front, rear and bogie respectively. The moments produced by suspension forces can be expressed as:

$$M_{susp1} = 2b^2K_{px}(-\psi_1 + \psi_b) + 2b^2C_{px}(-\dot{\psi}_1 + \dot{\psi}_b) \quad (11)$$

$$M_{susp2} = 2b^2K_{px}(-\psi_2 + \psi_b) + 2b^2C_{px}(-\dot{\psi}_2 + \dot{\psi}_b) \quad (12)$$

Where K_{px} is the longitudinal spring stiffness and C_{px} is the longitudinal damper coefficients.

6. Development of 1/5 scale roller rig model

Equations (1-6) were used to develop the model for 1/5 scaled bogie but with adjustments in the creepages developed at the contact patch due to the variation of velocity on the roller head and the minute longitudinal velocity introduced to the roller head when it is yawed. The scaling for this 1/5 scale roller rig model was achieved by using dimensional scaling. Some scaling imperfections might occur in the scaling of the modulus of rigidity and gravitational acceleration. Also the roller circumferential velocity was considered as an additional term to the lateral and spin creepages developed in the real railway wheel-rail contact patch during modelling based on the method described by Jaschinski et al [8]. The dynamic analysis of the roller rig behaviour concentrates on the displacements, velocities and acceleration of the various bodies and the forces between these bodies and the wheel-rail interface. The most common measurements in dynamic studies are made in the form of time histories of frequency spectra so it will be convenient if the simulated results for the scaled roller rig and the full size vehicle will show the same frequency components. However Jaschinski et al [8] mentioned that the scaling factor for time is equal to one while the rig dimensions are scaled down to one-fifth of the full scale vehicle model for the MMU scaled roller rig (which is considered as a case study in this paper).

Table 1 contains the relevant parameters for Full Scale model and 1/5 scale roller rig model where

$\alpha = 5$ for the scaled roller rig model.

Table 1. Full Scale Model and 1/5 Scale roller rig model parameters [8], [10].

Parameters	Full Scale Model	Scale	1/5 Scale roller rig
Wheelset mass m (kg)	1587.5	m/α^3	12.7
Bogie mass m_b (kg)	2612.5	m_b/α^3	20.9
Wheelset Yaw moment of inertia I_z (kgm^2)	1000	I_z/α^5	0.32
Bogie Yaw moment of inertia I_b (kgm^2)	3937.5	I_b/α^5	1.26
Lateral stiffness of primary suspension K_{py} (N/m)	4.5×10^6	K_{py}/α^3	36×10^3
Longitudinal primary suspension stiffness K_{px} (N/m)	12.5×10^6	K_{px}/α^3	100×10^3
Lateral damping of primary suspension C_{py} (Ns/m)	3.33×10^5	C_{py}/α^3	2.67×10^3
Longitudinal damping of suspension C_{px} (Ns/m)	1.51×10^6	C_{px}/α^3	12.05×10^3
Wheelbase b (m)	1.25	b/α	0.25
Wheel radius R_o (m)	0.5	R_o/α	0.1
Roller radius R_r (m)	0.5	R_r/α	0.18
Gauge l_o (m)	1.435	l_o/α	0.287

7. Simulated dynamic behaviour of 1/5 scale roller rig model and full scale rig model

The dynamic non-linear differential equations were reduced to first order equations and then solved using ode23 solver in MATLAB. This solver works out the stiff non-linear differential equations using Rosenbrock's method for solution of ordinary differential equations. The solver calculates the values for the following twelve state variables: $y_1, y_2, \dot{y}_1, \dot{y}_2, \dot{\psi}_1, \dot{\psi}_2, \psi_1, \psi_2, \dot{\psi}_b, \psi_b, y_b, \dot{y}_b$. The differential equations of the full scale model and the scaled roller rig model were solved with initial conditions given to the state variables.

Given the initial values of the lateral displacements, at low forward speeds, the wheelsets return to a central position hence the system is stable. As the forward speed increases, the wheelset lateral behaviour on the track becomes unstable and hunting results. The forward speed at which hunting occurs is referred to as the critical velocity of the vehicle. Figure 7 and figure 8 show the lateral behaviour of the wheelset for varying forward speeds on the railway bogie and a roller rig.

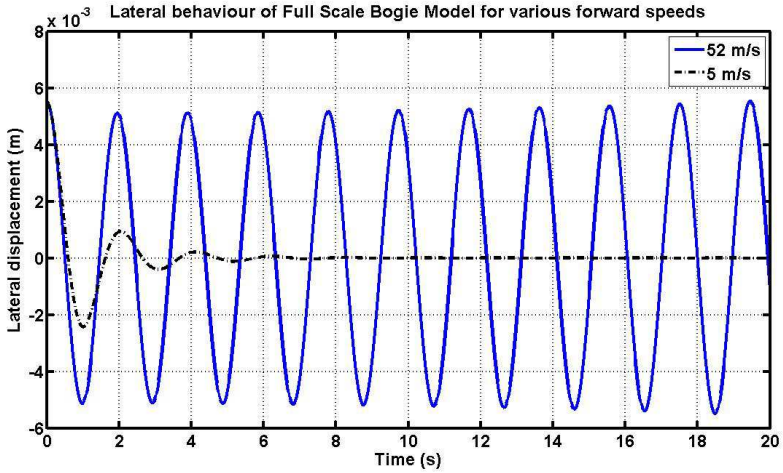

Figure 7. Lateral behaviour of the Full Scale bogie for various forward speeds.

Using the primary suspension parameters of the scaled roller rig and the full scale model, the

forward speed was gradually increased until flange contact with the rail gauge occurred. It is imperative to note that the flange clearance is given as 5.5 mm (0.0055m) as can be observed from the rolling radius difference function.

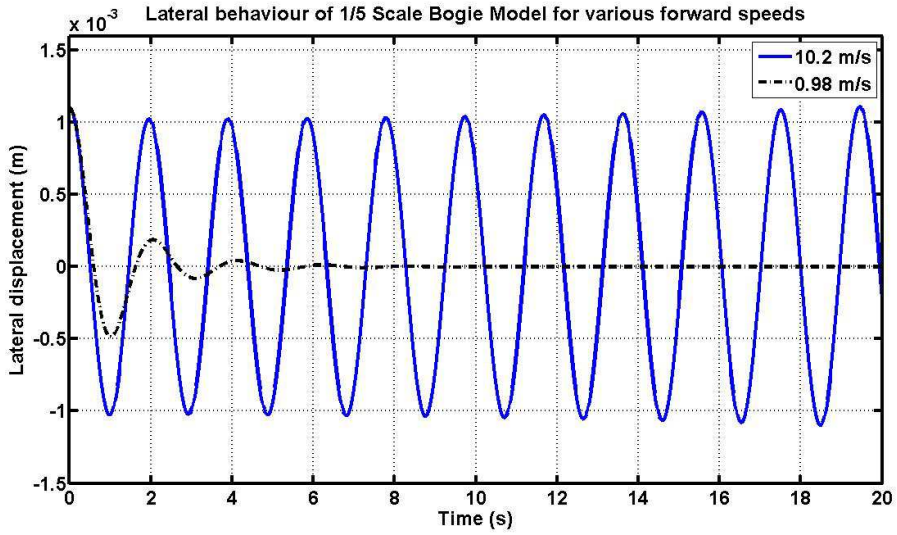

Figure 8. Lateral behaviour of the 1/5 Scale roller rig for various forward speeds.

The critical velocity at which hunting occurs for the full scale model was determined as 52 m/s while the critical velocity for the 1/5 scale roller rig was found to be 10.2 m/s. It can be observed from the simulations that the critical velocity of the 1/5 scaled roller rig model and the full scale model is related to the scale used. The critical velocity of the scale roller rig is approximately one-fifth of the critical velocity of the full scale roller rig.

8. Wear Modelling based on Archard's wear model

The wear model used for prediction is the Archard's wear model [3]. The wear prediction model is used to expose the wheel to contact scenarios that are most likely to be observed when travelling on a rail network or a certain route using simulations.

An initial wheel profile is used to develop the first version of the full scale roller rig model which contains the non-linear equations related to wheel-rail contact geometry, creep forces and suspension forces. The model is implemented in MATLAB and ode23 solver is employed. The simulated results give numerical values for lateral displacements, lateral velocities, yaw angles and yaw velocities of wheelset 1 and 2 on the track. Then the creep forces, lateral displacements, contact patch, creepages, normal contact forces are included in the KTH wear model. The MATLAB simulations generate the values for wear depth and wear volume, which are included in the first version of the full scale roller rig model. The resulting second version of the model is implemented in MATLAB again and the process continues until the time corresponding to the final distance is reached.

Dynamic time-domain simulations are carried out to simulate the behaviour of the bogie on the rollers or the full scale bogie on a track. The wheel-rail contact geometry, the wheel and rail profiles are all taken into consideration when modelling. The output of the dynamic wheel-rail/roller contact model then feeds into Wear model as inputs. The outputs of the wear model generate the worn rolling radius and worn wheel profile. It is imperative to note that the wear depth Δz is calculated at every time step and the worn rolling radius is computed by subtracting the wear depth from the rolling radius of the initial wheel profile design used for simulations. The wear step is continuously updated and repeated until the entire distance and total time is attained. The roller rig uses EN8 steel with the following chemical composition; 0.4% of carbon, 0.25 % silicon, 0.80% manganese, 0.015% sulphur

and 0.015 % phosphorus. Hardness property of EN8 steel (H) ranges from 500 N/mm^2 to 800 N/mm^2 [9].

According to Archard's wear model, the volume of worn material is directly proportional to the sliding distance, the normal force (N) and the wear coefficient (k) and is inversely proportional to the hardness of the worn material (H) [4].

$$V_{speed}(m^3) = \frac{ksN}{H} \tag{16}$$

The wear coefficient k can be calculated by computing the values of the slip velocity and then interpolating values with the contact pressure distribution, to compute the constant k. Table 2 contains the values of k obtained from three sets of experiments on a twin disc roller rig.

"Table 2. Wear coefficient (KTH function) [3].

Pressure p (GPa)	**Slip velocity v_{slip} (m/s)**	**k (10^{-4})**
p > 2.1	0 – 1	300 – 400
p < 2.1	v_{slip} < 0.2	1 – 10
p < 2.1	0.2 < v_{slip}<0.7	30 – 40
p < 2.1	v_{slip} < 0.7	1 – 10

The output from the dynamic simulations of the wheel-rail/roller contact model such as the semi axes of the contact patch, the maximum contact pressure, creepages and coefficient of friction is input into the Archard's wear model. FASTSIM algorithm [7] is applied to determine the slip velocity and the slip distance of the vehicle. According to Archard's model, wear does not occur in the adhesion region of the contact patch but the slip region only. This happens because at the adhesion region, the sliding distance is zero for all grid elements inside the contact patch. The elliptical contact patch is discretized using FASTSIM into 81 x 81 elements for accurate calculation of wear distributions. The slip velocity can be calculated as follows:

$$v_{slip} = V_{speed}\begin{bmatrix} v_x - v_{spin}y \\ v_y + v_{spin}x \end{bmatrix} \tag{17}$$

The magnitude of the slip velocity is calculated by taking the magnitude of the slip velocities in the longitudinal and lateral direction.

$$|v_{slip}| = \sqrt{V_x^2 + V_y^2} \tag{18}$$

where V is the forward vehicle speed, v_x is the longitudinal creepage, v_y is the lateral creepage, and v_{spin} is the spin creepage. The sliding distance S can be calculated as thus:

$$S = |v_{slip}|\frac{dx}{V_{speed}} \tag{19}$$

finally the total wear depth can be computed as follows:

$$\Delta z = k\frac{Sp}{H} \tag{20}$$

where Δz is the wear depth, *dx* is the longitudinal element and *k* is the wear coefficient and p is the contact pressure of each grid.

9. Simulated rolling radius using full scale model (which includes the wear prediction model)

For various forward speeds, the wear depth was calculated for 20 seconds simulation time. The depth of wear was subtracted from the initial rolling radius to determine the worn rolling radius. The rolling radius responses for the initial and worn wheel profiles for left and right wheels are shown in the following figures;

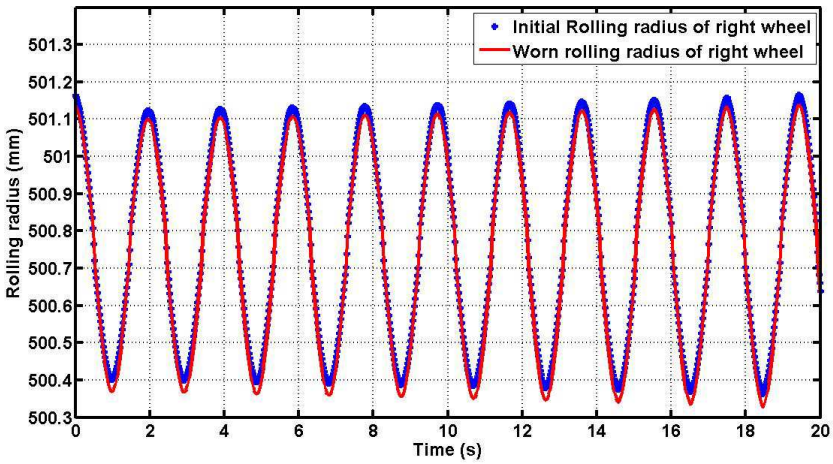

Figure 9. Simulated rolling radii for initial and worn profiles of the right wheel.

Figure 9 shows that the simulated values for the rolling radius function for initial and worn profiles of the right wheel present slight deviations. It is supposed that the wheel moves at critical speed 52 m/s.

The wear depth plot against distance travelled is shown in figure 10 below. It can be observed that wear depth increases with distance. At 772m the cumulative wear depth that is the average wear depth on the right wheel is 2.678 x 10^{-9} mm. This wear depth increases sharply from 0 m to 160 m and then increases steadily from 160 m to 772 m.

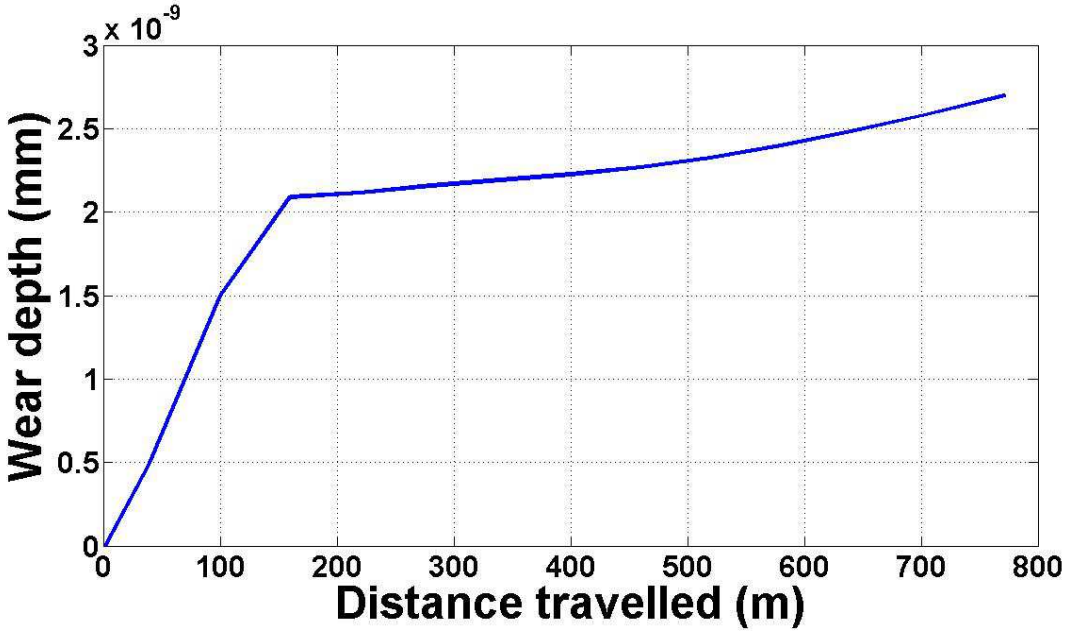

Figure 10. Simulated wear depth on the Right wheel.

It is important to note that the wear depth of the 1/5 scale roller rig is scaled down by 1/5th of the full wheel wear depth.

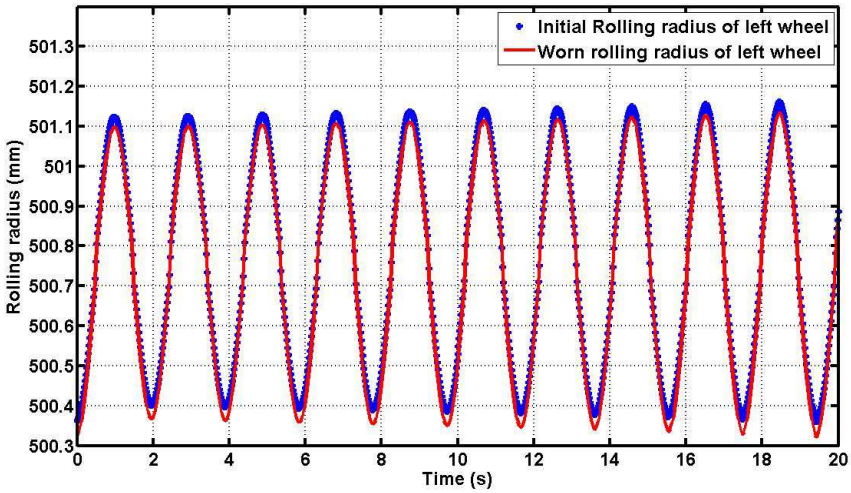

Figure 11. Simulated rolling radii for initial and worn profiles of the left wheel.

Figure 11 shows that the simulated values for the rolling radius function for initial and worn profiles of the left wheel present slight deviations. It is important to note that the starting rolling radius of the initial and worn wheel profile is different from that of the right wheel. This is due to symmetrical nature of the wheelset and the rolling radius difference function. The critical velocity of the wheelset is 52 m/s. The simulated wear depth result of the left wheel as a function of the travelled distance is shown in figure 12.

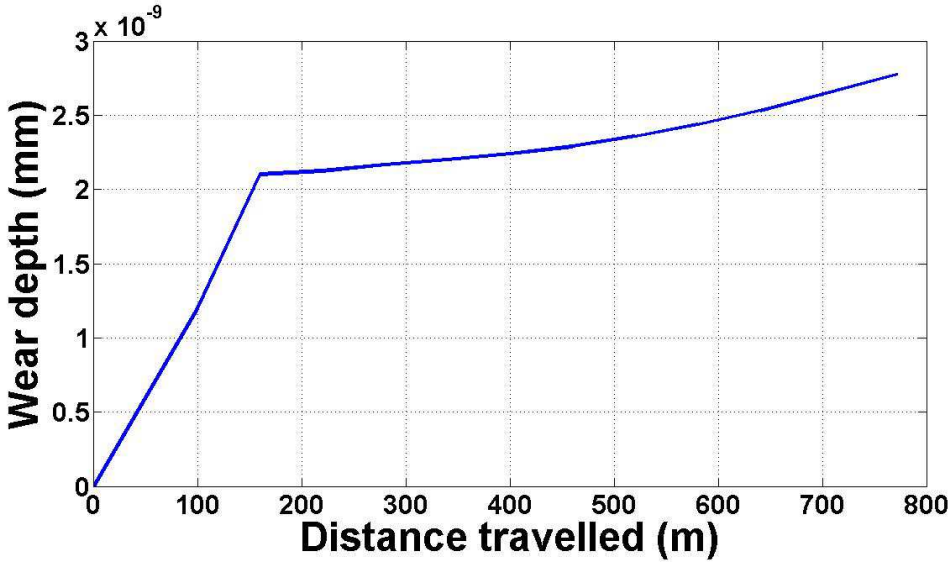

Figure 12. Simulated wear depth on the left wheel.

It can be observed that wear depth increases with distance. At 772m the wear depth on the right wheel is 2.778 x 10^{-9} mm. This wear depth increases sharply from 0 m to 160 m and then increases steadily from 160 m to 772 m.

Conclusion

This paper presents the modelling and simulation of the dynamic behaviour of full scale roller rig and 1/5 scale roller rig (including the wear prediction model based on KTH wear function).

The mathematical model for full scale rig was implemented in MATLAB. The wheel-rail contact geometry analysis comprising of the simulated results for wheel-rail profiles, contact point positions, radius difference function, contact angle function and equivalent conicity was discussed. The evaluation of wheel-rail contact forces using FASTSIM algorithm and wheelset suspension forces was performed and used in the dynamic simulation of the full scale roller rig model. The development of 1/5 scale roller rig model was also investigated. Results obtained from dynamic simulation of the 1/5 scale roller rig model compared well with the full scale model. It was observed that the critical velocity at which hunting occurs for the full scale roller rig model is 52 m/s while the scale roller rig model was 10.2 m/s.

A wear prediction model based on KTH wear function was used to investigate the influence of wear on the rolling radii of the left and right wheel profiles of the front wheel set. The simulated results showing the rolling radii for the full scale model with and without wear function are discussed. It is readily observed that the initial rolling radius of the wheelset decreases as it travels along the track due to wear

It can be concluded that the simulated critical speed for the 1/5 scale roller rig is about one-fifth of the critical speed for the full scale model and the rolling radius of the wheelset decreases as the wheelset travels on the track due to wear and the maximum value of the wear occurs in the wheel flange region. This paper presents the results of the initial stage of a large scale research project which concentrates on the influence of wear on the wheel-rail performance. Practical measurements of the critical speed and the wheels wear will be done using a scale roller rig and the simulated results will be compared with the experimental data in order to validate the proposed model.

References

[1] Hur H-M, Park J-H, Park T-W 2009 A study on the critical speed of worn wheel profile using a scale model *J. Mech. Sc and Tech* 23, pp. 2790-2800.

[2] Allen P. D, Iwnicki S. D 2001 The critical speed of a railway vehicle on a roller rig *Proc IMechE, Part F* 215 pp. 55 -64.

[3] Pombo J. Ambrosio Pereira M., Lewis R., Dwyce-Joyce R., Ariaudo C., Kuka N., 2011 Development of a wear prediction tool for steel railway wheels using three alternative wear functions *Wear* 271 pp. 238-245.

[4] Tomas J. 2002 Prediction of wheel profile wear—comparisons with field measurements *Wear* 253 pp. 89-99.

[5] Iwnicki S. 2003 Simulation of wheel–rail contact forces *Fatigue & Fracture of Engineering Materials & Structures* 26 pp. 887-900.

[6] Thomsen P G, True H. 2010 *Non-smooth Problems in Vehicle Systems Dynamics. Proc. Euromech 500 Colloquium* Springer.

[7] Vollebregt EAH., Wilders P. 2010 FASTSIM2: a second-order accurate frictional rolling contact algorithm *Computational Mechanics* 47 pp. 105-116.

[8] Jaschinski A., Chollet H., Iwnicki S., Wickens A., Würzen J. 1999 The Application of Roller Rigs to Railway Vehicle Dynamics *Vehicle Syst Dyn* 31 pp. 345-392.

[9] West Yorkshire Steel Ltd. 2011 EN8 steel - Technical Data. [online] http://www.westyorkssteel.com/en8.html [Accessed] 31 January 2012.

[10] Anyakwo A. Pislaru C. Ball A. Gu F. 2012 Dynamic simulation of a roller rig. In Proceedings of the 12th Conference on Computing and Engineering, University of Huddersfield. pp. 51-56.